The Journal of Physical Chemistry B

 VOLUME 103, NUMBER 4, JANUARY 28, 1999

LETTERS

Diffractive Optics-Based Heterodyne-Detected Grating Spectroscopy: Application to Ultrafast Protein Dynamics

Gregory D. Goodno,† Vladimir Astinov, and R. J. Dwayne Miller*

Departments of Chemistry and Physics, 80 Saint George Street, University of Toronto, Toronto, Ontario M5S 3H6, Canada

Received: August 28, 1998; In Final Form: November 23, 1998

The initial structural evolution of carboxymyoglobin (MbCO) following photodissociation of CO is measured using a recently developed method of heterodyne detection. This method increases the sensitivity, generates tilted pulse fronts which exactly cancel temporal broadening in noncollinear beam geometries, and provides an inherent acoustic reference that enables unambiguous separation of the real and imaginary components to the nonlinear susceptibility. With the latter advance, both the absorption anisotropy and its real counterpart, the phase anisotropy, can be measured with this technique. Access to the real part of the material anisotropy provides new information that can be correlated to the bath dynamics. In the MbCO studies, the phase anisotropy is found to develop on picosecond time scales and is much greater than can be attributed to the symmetry of the heme dipole transition. This provides direct evidence that the shape of the protein changes in the first few picoseconds following photodissociation. The asymmetric nature of the protein structure presumably plays an integral role in the development of the nonuniform displacements. The magnitude of the phase anisotropy and observed dynamics give strong evidence that the low-frequency collective modes of the protein are involved in transducing the reaction forces of the Fe ligation site into directed motions associated with the initial oxy to deoxy tertiary structure change.

I. Introduction

The heme protein carboxymyoglobin (MbCO) is often used as a model system for studying conformational relaxations in biological molecules, since interconversion between ligated and deligated structures can be conveniently triggered through photodissociation of the heme−ligand bond. Despite the attention that has been devoted toward MbCO,[1−11] the importance of the initial relaxation events following the bond break are still actively debated. It is clear that proteins have complex potential-energy surfaces in which there are a multitude of local minima corresponding to different conformations.[1−3] Since there are various length scales to the protein's motions and an associated barrier distribution, the protein relaxation exhibits highly nonexponential dynamics extending over many decades in time. The relaxation process is often modeled with stretched exponential functions with various assumptions about the connectivity of the dynamics to the barrier distribution.[4−6] This aspect of the protein relaxation could be referred to as the long-time dynamics. In contrast, it has recently been discovered that a significant fraction of the protein relaxation occurs within the first few picoseconds.[4,7−11] These early motions deviate from the monotonic predictions for the long time behavior. For example, the photoinitiated reaction forces lead to the displacement of acoustic-like modes of the protein that account for most of the initial protein strain.[7,10] Similarly, the largest shift in various spectral markers of protein relaxation occur on com-

† Department of Physics and Astronomy, University of Rochester, Rochester, NY 14627.

10.1021/jp983649n CCC: $18.00
Published on Web 01/13/1999

parable time scales.[4,9,12] The short and long time dynamics are related through fluctuation and dissipation processes, and it is possible to make a connection from the long time dynamics to reasonably short time scales within a model for the barrier crossing between configurations.[6] In analogy with analytic treatments of the inertial contributions to solvent relaxation dynamics,[13,14] this picosecond phase of the protein relaxation is best described within a modal basis.[10,15] Since the globin structure has low spatial symmetry, one would expect that the modes of the protein activated by the forces generated from the bond break should be nonuniform in their directionality—displacements of atoms along one direction will not be mirrored by displacements along another. If the short time dynamics play a relevant role in the conversion between ligated and deligated structures, one should be able to observe the development of anisotropic protein strain that would correspond to a degree of mode-selective coupling. We have recently observed the anticipated anisotropic displacements using transient grating (TG) spectroscopy and found them to be dominated by the short time dynamics.[10]

In this letter, we extend our previous grating studies of MbCO through the novel implementation of optical heterodyne detection (OHD) using diffractive optics.[16] This technique, when combined with polarization-selective methods, allows us to measure the anisotropic response of the protein in both phase and amplitude, corresponding to changes in the real and imaginary components of the index of refraction, respectively. The imaginary component is equivalent to the change in absorption at the probe wavelength that would be measured in a typical pump−probe experiment. The real component depends on the change in absorption as well through a Kramers−Kronig transform but also contains a contribution from global changes in the protein structure. By examining the anisotropy of both of these components in light of the known planar symmetry of the heme dipole transition, we can separate the protein structural changes from electronic contributions and infer information on the anisotropic protein motions on ultrafast time scales.

II. Experimental Technique

The basic method of performing OHD TG experiments using a diffractive optical element (DOE) has been presented elsewhere.[11,16−18] The signal-amplifying capability of this implementation has recently been confirmed independently by others as well.[19] The advantages of this technique are (1) passive phase stability between the input fields (<5° phase noise[16]) which eliminates the need for active phase locking; (2) automatic beam alignment for Bragg-angle phase matching[20] as well as automatic spatial and temporal overlap of the signal and reference pulses on the detector; (3) generation of tilted wave fronts, preserving the temporal and spatial resolution between the object and image plane (vide infra);[11] (4) high efficiency, comparable to conventional beam splitters, which is important in avoiding nonlinear effects in the diffractive optic itself;[11,16] and (5) straightforward extension to fifth-order nonlinear spectroscopies, where active phase-locking of six optical fields becomes prohibitively complex. Here we will focus on the salient details of this method with regard to measurement of the MbCO response.

The experimental setup is shown in Figure 1. A ∼100-fs, 400-nm pump pulse is spatially overlapped with a variably delayed, 800-nm probe pulse on the surface of a DOE, which splits each into two replicas (±1 diffractive orders; all other orders are spatially filtered). The resulting four pulses are achromatically imaged onto the sample by an Al-coated

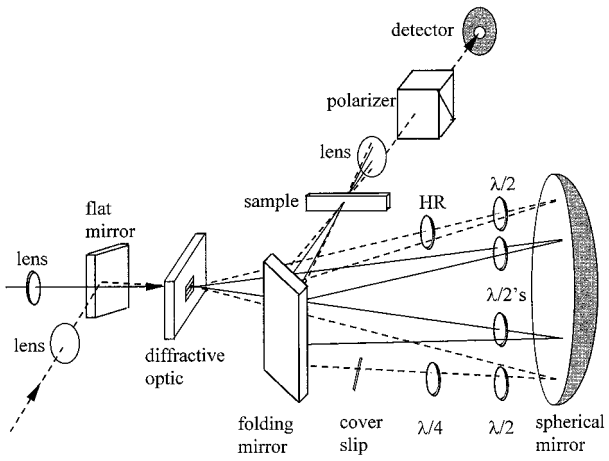

Figure 1. Experimental setup for polarization-resolved heterodyne-detected transient grating experiments: (- - -) 800 nm beams; (—) 400 nm beams. There is a delay line in the 800 nm beam path before the DOE that is not shown in this figure.

spherical mirror placed at a 1:1 conjugate ratio and tilted slightly off-axis (∼1°) to separate the incident and reflected beams. The two pump replicas overlap at an angle in the sample, forming a holographic interference pattern. The protein is photodissociated in the illuminated fringes and unchanged in the dark fringes, so that the complex index of refraction varies between them. One of the replicas of the 800-nm probe pulse is Bragg-diffracted from this photoinduced grating into the detector. The other 800-nm pulse replica passes through the sample and overlaps with the diffracted signal field on the detector to provide a reference field for OHD. The phase difference between the signal and reference fields can be adjusted by tilting a cover slip in the probe beam path, so that both the real and imaginary components of the change in the complex index can be measured. The reference intensity is attenuated by a factor of $\sim 10^3$ by a broad-band high-reflector mirror to optimize the signal-to-noise ratio[21] and avoid saturating the detector. Half-wave plates in each of the beam paths allow independent adjustment of all four field polarizations. Additional glass (not shown in Figure 1) is placed in the beam paths as necessary to overlap the time delays between the two pump pulses and between the probe and reference pulses.

The imaging setup of Figure 1 bears some analogy with the typical 4*f* imaging system used in Fourier optics for image processing and pulse shaping.[22,23] Like the 4*f* system, the setup used here has a delta-function impulse response function,[22] which means that the spatial field distribution at the object plane (the DOE) is perfectly reconstructed at the image plane (the sample position). A consequence of this property is that the time resolution and spatial overlap between the pump and probe pulses at the DOE is preserved at the sample position, even for very large spot sizes and diffraction angles. This feature is illustrated in Figure 2, which compares a standard pump−probe geometry for the overlap between two short laser pulses using a conventional beam splitter (Figure 2a) to the geometry using a DOE (Figure 2b). Since the spatial pulse envelopes immediately following the DOE are unchanged from the incident envelope, the wave fronts of the diffracted pulse are tilted with respect to the pulse envelope. Typically, geometric smearing of the time resolution occurs in noncollinear beam arrangements due to variations in the pulse propagation time across the transverse width of the laser beam.[24] When combined with an appropriate imaging setup (e.g., Figure 1), the tilted phase fronts generated by the DOE eliminate this source of temporal broadening. This key point with respect to implementing

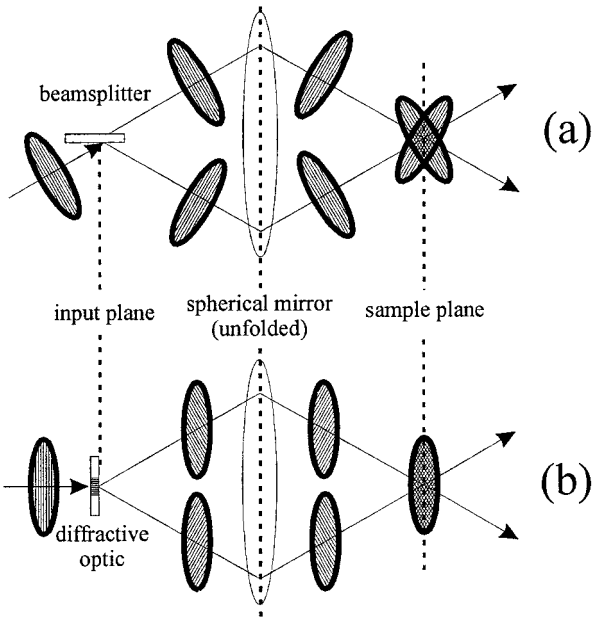

Figure 2. (a) Typical pump−probe geometry using a conventional beam splitter to generate the two pulse replicas. (b) Generation of pulse replicas with tilted wave fronts using a DOE instead of a beam splitter. This arrangement eliminates the geometric smearing of the time delay that is present in a. The ovals represent a snapshot of the spatial pulse envelope at a given instant in time, and the parallel lines inside the ovals represent the wave fronts.

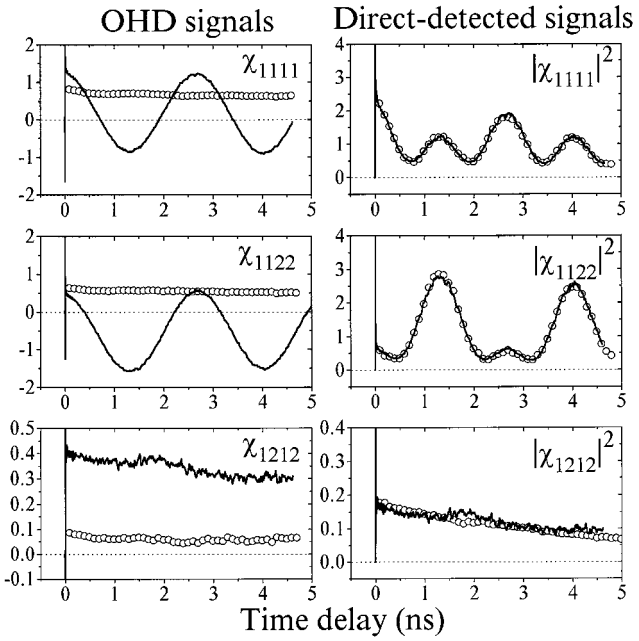

Figure 3. (Left) Optical heterodyne-detected transient grating signals from MbCO: (—) Re[χ_{ijkl}]; (○) −Im[χ_{ijkl}]. In our notation, the indices of the third-order susceptibility tensor element χ_{ijkl} refer to the polarizations of the two pump fields (*i*, *j*), the probe field (*k*), and the signal field (*l*). (Right) Comparison of the scaled direct-detected grating signals (○) to Re[χ_{ijkl}]^2 + Im[χ_{ijkl}]^2 (—).

femtosecond studies has been made earlier[11] and is readily appreciated from Figure 2. As an example, given the spot sizes and angles of incidence (200 μm and 15°, respectively) in the present experiments, the time resolution at the sample using the DOE improved from ∼150 to ∼100 fs, limited only by the incident pulse width.

This method can be used to improve the time resolution in noncollinear geometries for any experimental configuration (e.g. pump−probe, photon echo, etc.) by blocking the unwanted diffractive orders or by using a custom DOE. As this technique can be implemented using a reflection grating rather than a transmissive element, the time resolution should be limited only by the spectral amplitude filtering of the DOE; there are no spectral phase distortions imposed by this method. Assuming a Gaussian intensity fwhm spectral band-pass of $\Delta\omega$ for the DOE, the temporal broadening δT of the intensity envelope for Gaussian pulses centered at the same frequency as the DOE band-pass can be shown to be

$$\delta T = (\Delta T^2 + 32 \ln 2/\Delta\omega^2)^{1/2} - \Delta T \qquad (1)$$

where ΔT is the input pulse width (intensity fwhm). With the measured spectral band-pass of $\Delta\omega \approx 3$ rad/fs for the DOE used in this work, this gives an estimated 0.12 fs of broadening for 10-fs input pulses owing to spectral filtering. Thus, this optical setup may be useful for reducing geometric distortions in the measurement of very short (<10 fs) optical pulses[24] and offers significant advantages for preserving femtosecond time resolution in all classes of noncollinear spectroscopies.

III. Results and Discussion

For the MbCO data, the real (Re) and imaginary (Im) signal components were identified based on the presence or absence, respectively, of photoacoustic oscillations on nanosecond time scales. These sinusoidal oscillations in the signal arise from a standing acoustic wave that is created by both thermal expansion of the solvent as well as global structure changes in the protein.[7] Since these waves are simply density fluctuations of the solvent, to a good approximation they change only the real part of the refractive index. With this in mind, we set the phase difference between the input fields by tilting the cover slip in the probe beam to eliminate the acoustics, so that the observed signals were proportional to the Im component of the protein response. The Re component was measured separately by rotating a quarter-wave plate in the probe beam by 90° to interchange the fast and slow axes and thus impose a π/2-phase shift on the probe. Each trace (Re or Im) was taken to be the difference of two data sets acquired with a π-phase shift between them in order to eliminate residual direct-detected signals and (small) pump−probe modulations of the reference field as it passes through the photoexcited sample.[11] The sign of this pump−probe modulation establishes an absolute reference point for the phase difference of the input fields that indicates the signs of both the Im and Re components.

The OHD TG signals measured from 1 mM aqueous MbCO solutions are shown in Figure 3 (left side) for all relevant polarization configurations. As a consistency check, the Re and Im components for each tensor element of the MbCO response were squared and added together for comparison with the direct-detected signals measured with the reference beam blocked. As shown in Figure 3 (right side) the agreement between these is excellent, demonstrating that the Re and Im traces are linear in the signal field and in quadrature with one another.

The most interesting features of the initial protein response can be highlighted by constructing the absorption and phase anisotropies $r_{Im}(t)$ and $r_{Re}(t)$ from the measured data by extending the standard definition for pump−probe experiments[25] to the grating signals:[26]

$$r_{Re}(t) \equiv \frac{\mathrm{Re}[\chi_{1111}(t)] - \mathrm{Re}[\chi_{1122}(t)]}{\mathrm{Re}[\chi_{1111}(t)] + 2\mathrm{Re}[\chi_{1122}(t)]} \qquad (2a)$$

$$r_{\mathrm{Im}}(t) \equiv \frac{\mathrm{Im}[\chi_{1111}(t)] - \mathrm{Im}[\chi_{1122}(t)]}{\mathrm{Im}[\chi_{1111}(t)] + 2\mathrm{Im}[\chi_{1122}(t)]} \qquad (2b)$$

The anisotropy is essentially a normalized measure of the difference in the optical properties of the material for probe fields polarized parallel or perpendicular to the pump field. The dipole transitions at the pump (400 nm) and probe (800 nm) wavelengths are dominated by the heme, which is known to be a circularly symmetric (planar) absorber in the Soret band (420 nm) with a theoretical anisotropy of 1/10.[27] As can be seen from Figure 4, the absorption anisotropy $r_{\mathrm{Im}}(t)$ is roughly constant at $0.09^{+0.03}_{-0.07}$ after $t = 5$ ps. This final value is in qualitative agreement with measurements made for probe wavelengths in the Soret band[28] and in band III (760 nm),[10] although the large uncertainty in our measurements precludes a quantitative comparison. The uncertainty in the absolute magnitude of $r_{\mathrm{Im}}(t)$ arises from small uncalibrated changes in the probe amplitude ($\sim$5−10%) for the different settings of the quarter-wave plate used to acquire the Re and Im components. This uncertainty propagates to the relative amplitudes of $\mathrm{Im}[\chi_{1111}(t)]$ and $\mathrm{Im}[\chi_{1122}(t)]$, such that the final value of $r_{\mathrm{Im}}(t)$ could lie between 0.02 and 0.12. This systematic uncertainty is not present in $r_{\mathrm{Re}}(t)$, since the amplitude of the photoacoustics provides an absolute calibration standard between the Re components of the tensor elements. A definitive interpretation of $r_{\mathrm{Im}}(t)$ must await a more quantitative measurement (in progress),[29] but it is nevertheless clear from these data that the electronic state relaxation is essentially complete within several picoseconds, in agreement with previous pump−probe studies.[4,9,10]

The most intriguing results of this work are the observed magnitude and dynamics of the phase anisotropy $r_{\mathrm{Re}}(t)$, which can be seen from Figure 4 to be remarkably different than those of its absorption counterpart. The observed phase anisotropy develops on a 15 ps time scale and attains a final value of 0.37 ± 0.02. This is much larger than can be attributed to the contribution from the electronic state change between MbCO and deoxyMb. It can be shown from a Kramers−Kronig transform[29] of the anisotropic equilibrium difference spectra of MbCO and deoxyMb[27,30,31] that the relaxed (>10 ps) value of the phase anisotropy from the electronic state change is 0.17 ± 0.01. Thus, the observed magnitude and dynamics of $r_{\mathrm{Re}}(t)$ must arise from contributions other than electronic relaxation. The most likely source is anisotropic strain in the protein lattice.

From geometric considerations of the photoselected orientational distribution of excited molecules, it is straightforward to relate the measured grating signals to the components of the molecular index ellipsoid within and perpendicular to the heme plane.[29,32] A clear result from the data in Figure 3 is that the net in-plane and out-of-plane index changes are positive and negative, respectively. The sign of the index change is opposite the sign of the molecular strain (relative atomic displacements),[10] so it can be inferred that the protein is expanding along the direction perpendicular to the heme plane and contracting within the plane of the heme. By comparing the sign of the acoustic wave launched by the protein volume change to the sign of the thermally driven wave, it has been shown previously that the protein undergoes a net contraction upon conformational relaxation.[7] Thus, the net magnitude of the in-plane contraction is greater than the out-of-plane expansion. By solving for the in-plane and out-of-plane contributions to the different tensor elements,[29] we have found that the net index change in-plane is reasonably well described with a 4 ± 2 ps time constant in agreement with our earlier work[10] whereas the perpendicular component has a characteristic time constant of 12 ± 3 ps and

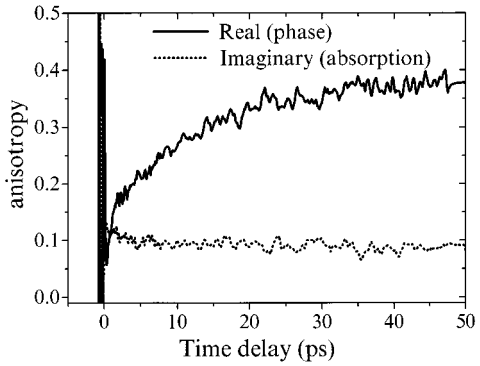

Figure 4. Absorption anisotropy $r_{\mathrm{Im}}(t)$ and phase anisotropy $r_{\mathrm{Re}}(t)$ constructed from the data in Figure 3 according to eq 2. The greatly different magnitude and dynamics between these two traces indicate there is a nondipole contribution to $r_{\mathrm{Re}}(t)$.

is of the opposite sign. These dynamics are not observed in studies of the photodissociation of heme-CO, which provides a control for the dipole contribution to the phase anisotropy without the protein present. Further control studies are needed to provide a definitive explanation for the increase in the phase anisotropy seen in Figure 4. These dynamics most likely include contributions from thermal relaxation of the hot protein as well as anisotropic strain in the protein lattice. The large difference in the time constants for the in-plane and out-of-plane index changes suggests that anisotropic protein strain is a major contributor to the grating signals. This connection to the anisotropic protein contributions was not possible in our previous studies[10] as such information is only retrievable with the new heterodyne capabilities to linearize the signal and eliminate absorptive contributions.

From the current findings, the protein's anisotropic relaxation is virtually complete within 15 ps. There may be longer components, but within the rotational diffusion time scale (10 ns), the short time protein response clearly dominates. The global nature of the index of refraction changes and the observed dynamics are compelling evidence that low-frequency collective modes of the protein play an important role in directing the reaction forces to specific motions important to function. The fast change in the shape of the protein indicates that the reaction forces couple most strongly to a few specific modes, rather than activating a contiguous distribution. Mode-specific coupling is undoubtedly a consequence of the underlying asymmetry in the protein structure and excited-state potential surface, which funnels the small amount of input energy liberated by the bond break into orientationally specific displacements. This concept of spatially directed reaction forces is embedded in the allosteric core model for the communication pathway between heme proteins in hemoglobin[33] and should be a common feature of all biochemical reactions involving proteins where mesoscopic changes in molecular conformations are part of the functional response. While it is clear that the structural evolution continues over a range of time scales out to microseconds and longer,[1−6] the protein architecture is such that the collective displacement of specific modes guides the system along the correct seam in the potential surface and greatly constrains the reaction phase space to efficiently transduce the reaction forces to functionally relevant structure changes.

Note: In a very recent paper published after this manuscript was submitted,[34] Nelson and co-workers independently demonstrated the overlap of ultrashort pulses using an optical setup similar to the one described here and in our previous work.[11]

Acknowledgment. This research was supported by the Natural Sciences and Engineering Research Council of Canada and Photonics Research Ontario.

References and Notes

(1) Frauenfelder, H.; Parak, F.; Young, R. D. *Annu. Rev. Biophys. Biochem*. **1988**, *17*, 451. Frauenfelder, H.; Sligar, S. G.; Wolynes, P. G. *Science* **1991**, *254*, 1598.

(2) Fritsch, K.; Friedrich, J.; Parak, F.; Skinner, J. L. *Proc. Natl. Acad. Sci. U.S.A.* **1996**, *93*, 15141. Leeson, T.; Wiersma, D. A. *Phys. Rev. Lett*. **1995**, *74*, 2138.

(3) Leeson, D. T.; Wiersma, D. A.; Fritsch, K.; Friedrich, J. *J. Phys. Chem.* **1997**, *101*, 6331.

(4) Lim, M.; Jackson, T. A.; Anfinrud, P. A. *Proc. Natl. Acad. Sci. U.S.A.* **1993**, *90*, 5801.

(5) Sage, J. T.; Schomacker, K. T.; Champion, P. M. *J. Phys. Chem*. **1995**, *99*, 3394.

(6) Hagen, S. J.; Eaton, W. A. *J. Chem. Phys*. **1996**, *104*, 3395.

(7) Genburg, L.; Richard, L.; McLendon, G.; Miller, R. J. D. *Science* **1991**, *251*, 1051.

(8) Miller, R. J. D. *Acc. Chem. Res.* **1994**, *27*, 145.

(9) Franzen, S.; Bohn, B.; Poyart, C.; Martin, J. L. *Biochemistry* **1995**, *34*, 1224.

(10) Deak, J.; Chiu, H. L.; Lewis, C. M.; Miller, R. J. D. *J. Phys. Chem.* **1998**, *102*, 6621.

(11) Dadusc, G.; Goodno, G. D.; Chiu, H. L.; Ogilvie, J.; Miller, R. J. D. *Israel J. Chem.* **1998**, *38*, in press.

(12) Friedman, J. M.; Scott, T. W.; Fisanick, G. J.; Simon, S. R.; Findsen, E. W.; Ondrias, M. R.; Macdonald, V. W. *Science* **1985**, *229*, 187.

(13) Cho, M.; Fleming, G. R.; Saito, S.; Ohmine, I.; Stratt, R. M. *J. Chem. Phys.* **1994**, *100*, 6672.

(14) Keyes, T. *J. Chem. Phys.* **1994**, *101*, 5081.

(15) Seno, Y.; Go, N. *J. Mol. Biol*. **1990**, *216*, 111.

(16) Goodno, G. D.; Dadusc, G.; Miller, R. J. D. *J. Opt. Soc. Am. B* **1998**, *15*, 1791.

(17) Goodno, G. D.; Miller, R. J. D. In *International Quantum Electronics Conference*; 1998 OSA Technical Digest Series; 1998, Vol. *7*, p 101.

(18) Goodno, G. D.; Astinov, V.; Miller, R. J. D. In *Ultrafast Phenomena XI*; Springer-Verlag: Berlin, in press.

(19) Maznev, A. A.; Nelson, K. A.; Rogers, J. A. *Opt. Lett.* **1998**, *23*, 1319.

(20) Rogers, J. A.; Nelson, K. A. *Physica B* **1996**, *219&220*, 562.

(21) Levenson, M. D.; Eesley, G. L. *Appl. Phys.* **1978**, *19*, 1.

(22) Saleh, B. E. A.; Teich, M. C. *Fundamentals of Photonics*; John Wiley & Sons: New York, 1991.

(23) Weiner, A. M.; Oudin, S.; Leaird, D. E.; Reitze, D. H. *J. Opt. Soc. Am. A* **1993**, *10*, 1112.

(24) Taft, G.; Rundquist A.; Murnane, M. M.; Christov, I. P.; Kapteyn, H. C.; DeLong, K. W.; Fittinghoff, D. N.; Krumbugel, M. A.; Sweetser, J. N.; Trebino, R. *IEEE J. Sel. Top. Quantum Electron.* **1996**, *2*, 575.

(25) Magde, D. *J. Chem. Phys.* **1978**, *68*, 3717.

(26) Myers, A. B.; Hochstrasser, R. M. *IEEE J. Quantum Electron.* **1986**, *22*, 1482.

(27) Eaton, W. A.; Hofrichter, J. *Methods Enzymol.* **1981**, *76*, 175.

(28) Ansari, A.; Jones, C. M.; Henry, E. R.; Hofrichter, J.; Eaton, W. A. *Biophys. J.* **1993**, *64*, 852.

(29) Goodno, G. D.; Astinov, V.; Miller, R. J. D. Manuscript in preparation.

(30) Churg, A. K.; Malkinen, M. W. *J. Chem. Phys.* **1978**, *68*, 1913.

(31) Eaton, W. A.; Hanson, L. K.; Stephens, P. J.; Sutherland, J. C.; Dunn, J. B. R. *J. Am. Chem. Soc.* **1978**, *100*, 4991.

(32) Kliger, D. S.; Lewis, J. W.; Randall, C. E. *Polarized Light in Optics and Spectroscopy*; Academic Press: San Diego, CA, 1990.

(33) Gelin, B. R.; Karplus, M. *Proc. Natl. Acad. Sci. U.S.A.* **1977**, *74*, 801.

(34) Maznev, A. A.; Crimmins, T. F.; Nelson, K. A. *Opt. Lett.* **1998**, *23*, 1378.